Detection of extremely weak NQR signals using stochastic resonance and neural network theories

Weihang Shao, Jamie Barras, Panagiotis Kosmas

PII: S0165-1684(17)30237-2
DOI: 10.1016/j.sigpro.2017.06.027
Reference: SIGPRO 6526

To appear in: *Signal Processing*

Received date: 18 March 2017
Revised date: 6 June 2017
Accepted date: 27 June 2017

Please cite this article as: Weihang Shao, Jamie Barras, Panagiotis Kosmas, Detection of extremely weak NQR signals using stochastic resonance and neural network theories, *Signal Processing* (2017), doi: 10.1016/j.sigpro.2017.06.027

HIGHLIGHTS

- The proposed SRNN method is a combination of stochastic resonance and neural network, which effectively detects extremely weak NQR signals.
- The SRNN method can detect a variety of NQR signals which have similar NQR parameters, which shows SRNNs good commonality, as well as robustness to the possible time-variation of NQR signal properties in real life settings.
- The SRNN method also has good performance in the presence of interference.
- We anticipate that the proposed SRNN method can be applicable to other problems of detecting weak signals under a similar framework.

Detection of extremely weak NQR signals using stochastic resonance and neural network theories

Weihang Shao,[1] Jamie Barras,[1] and Panagiotis Kosmas[1]

[1]*Department of Informatics, King's College London*

(Dated: July 11, 2017)

Abstract

Nuclear Quadrupole Resonance (NQR) signal detection is widely used for searching related substances of interest, such as explosives, petroleum, drugs, etc. NQR responses from these substances are usually very weak compared to background noise. Moreover, in some applications such as landmine detection, NQR responses decay with time quickly, and the required scanning times are usually prohibitively long. This paper presents a novel approach which can detect NQR signals of very low SNRs in such scenarios, by combining a stochastic resonance framework and neural network theory. Firstly, the approach relies on the design of a stochastic resonance (SR) system which can transform the original data into a nonlinear waveform with special SR features. Secondly, a (feedforward) robust neural network is trained to discern this nonlinear waveform accurately, in order to identify the NQR signal. Our results demonstrate that the neural network approach outer-performs traditional signal processing detection and estimation methods. Moreover, this stochastic resonance neural network approach (SRNN) can be designed to detect a variety of NQR signals which have similar NQR parameters but not identical resonant bands. The SRNN approach can also be effective in cases where both noise and radio frequency interference are strong relative to the NQR response.

I. INTRODUCTION

Quadrupolar nuclei can resonate when probed by external electromagnetic (EM) waves, producing a response known as the nuclear quadrupole resonance (NQR) signal [1]. Based on this principle, NQR signal detection is a useful technique for identifying the presence of substances containing quadrupolar nuclei. Its applications include landmine and drug detection, medicine authentication, security checking, oil drilling, etc, [2–4], for which resonant quadrupolar nuclei always exist in compounds of the objects of interest (such as the ^{14}N of trinitrotoluen, aka TNT, in landmines).

In many applications, the NQR signal that is due to the substance of interest suffers from a very low signal to noise ratio (SNR), and thus cannot be detected by traditional spectrum analysis methods. To increase SNR during data acquisition, one can use an "echo train" technique based on pulsed spin locking sequences [5, 6], which can maintain the intensity of the NQR signal by echoing/restoring the NQR signal periodically. The system can therefore record sufficiently long data before full relaxation, thereby providing a straightforward and useful strategy for increasing the SNR. Since each echo not only restores the intensity but also the initial phase of the NQR signal, summing up all data echoes will result in the NQR signal added coherently as opposed to the stochastic noise with its random phase. The echo train, however, suffers from an important limitation, as it may require prohibitively long times for data collection in applications such as humanitarian demining and security checking.

For this reason, researchers have relied on least squares estimation or maximum likelihood theory to identify the NQR signal by estimating parameters which depend on the source substance, such as frequency, signal damping time, and echo decay time. These parameter estimation algorithms proposed in recent years are to some extent robust to low SNR cases, but suffer from the effect of strong radio frequency (RF) interference [7, 8]. Our recent work on this topic has proposed significant improvements to enhance detection in cases of strong RF interference [9, 10]. However, these interference-cancellation algorithms still rely on the approximate maximum likelihood theory approach of [7] and [8] to deal with noise, which requires SNR levels that are higher than those considered in this work and in many realistic applications.

A completely different approach to increase the SNR can be adopted based on stochastic resonance (SR) theory, by which a weak signal immersed in strong stochastic noise background can be considerably magnified [11, 12]. Even for very low SNR cases, the original signal will resonate

with the stochastic noise resulting in a signal which contains a strong frequency component of the signal of interest, and thus a higher SNR than the original data. Therefore, our aim is to incorporate a SR system into the echo train spectrometer, which can allow substance identification even in cases of extremely weak NQR signal levels. After the signal passes through the SR system, a detection algorithm is needed to process the resulting nonlinear time-domain waveform. In addition to the resonant signal of interest, this waveform will contain resonant stochastic noise components which can cause false alarms (see the discussion in Section III and Fig. 4). To overcome this challenge, we apply a neural network (NN) method [13], which is shown to be suitable for discerning waveforms corresponding to NQR signals from the total data. The proposed method is termed as SRNN, as it combines SR and NN theories.

The remainder of the paper is structured as follows. In the next section, we introduce the SR system implementation and present possible algorithms applied to the SR system output data for NQR detection, including the previously reported AML and FSAML in addition to the new NN method. We use numerical data to compare performance among various NQR detection methods in Section III, and show that the SRNN method outer-performs previously proposed algorithms in detecting signals with low SNRs. We also show that the NN implementation can be applied to detect not only a specific NQR signal, but also a variety of NQR signals with NQR parameters within a specified range. Finally, we show how the NN method can be adapted to deal successfully with cases where interference is also strong and obscures the signal further than the high noise level. Conclusions are given in the last section.

II. THE SR SYSTEM AND ITS COMPANION ALGORITHM

A. Applying an SR model to the NQR signal

We consider an NQR signal with only one resonant frequency. It can be written, during one echo time, as [14],

$$y(t) = \alpha \cos\left(2\pi \check{f} t + \varphi\right) e^{-|t-t_{sp}|/T^*}, \tag{1}$$

where $t=t_0,...,t_{N-1}$ is the N-points echo sampling time with the symmetric center to be t_{sp}, and α, T^*, $\check{f}$, and φ are the amplitude, damping time, frequency, and initial phase of NQR signal, respectively. Assuming a Gaussian white noise background, the NQR data $z(t)$ can be written as

$$z(t) = y(t) + n(t), \tag{2}$$

where $n(t)$ is Gaussian noise of zero mean and D distribution variance. The signal to noise ratio (SNR) of this data is [11],

$$\mathrm{SNR} = 20\lg\left(\frac{\pi}{4}\cdot\frac{\bar{\alpha}^2}{D}\right), \tag{3}$$

where

$$\bar{\alpha} = \frac{1}{2t_{sp}}\int_0^{2t_{sp}} \alpha e^{-|t-t_{sp}|/T^*}\mathrm{d}t = \frac{T^*}{t_{sp}}\alpha\left(1-e^{-t_{sp}/T^*}\right), \tag{4}$$

is the average NQR signal amplitude during one echo.

As mentioned in the Introduction, even if we sum data from all echoes to achieve a relatively higher SNR, noise can be inevitably strong for detection, i.e. $D \gg \alpha^2$. For these cases, we propose to design an SR system which can transform the original NQR data z to a waveform of detectable NQR signal characteristics x. The function of this system can be mathematically written as,

$$\frac{dx}{dt} = c_1 x - c_2 x^3 + z, \tag{5}$$

where z, x are the SR system's input and output, respectively, and c_1 and c_2 are constant coefficients of this system. To achieve strong resonance, the values of c_1 and c_2 should approximately satisfy

$$\frac{c_1}{2\pi\sqrt{2}}e^{-\frac{c_1^2}{2c_2 D}} \simeq \check{f}, \tag{6}$$

according to the Kramers's theory [15, 16]. In fact, $\check{f} \simeq \frac{c_1}{2\pi\sqrt{2}}$ as D is large enough for low SNR data. We note that x cannot be acquired by sampling z and solving Eq. (5) mathematically, because discrete sampling data cannot provide sufficient precision for this approach. The SR system should therefore be a hardware implementation which can sample z continuously, *e.g.*, an integration circuit [11, 12]. To simulate this SR system, we need to consider a thermal fluctuation time τ for the noise, *i.e.*, the noise remains unchanged during the time interval τ. The range of τ is about 1ns$\sim$1μs according to thermodynamic theory [17]. Then Eq. (5) can be precisely solved using a strategy based on 4-order Runger-Kutta method (see the Appendix for more details).

By choosing c_1 and c_2 appropriately, the solution to the SR model described by Eq. (5) can guarantee that the output x can always fluctuate around a certain periodic nonlinear waveform (the output of no noise case, *i.e.*, D=0) regardless of the noise amount. The example in Fig. 1 shows that the SR system can result in the (very weak) NQR signal (see bottom plot) being a distinct nonlinear waveform (top plot), where c_1=10 and c_2=0.5.

Although numerical tests show that when $\tau \to 0^+$, the fluctuation $\to 0$, in reality, for the short time and radio frequency NQR signal, τ is usually not small enough to restrict the fluctuation which

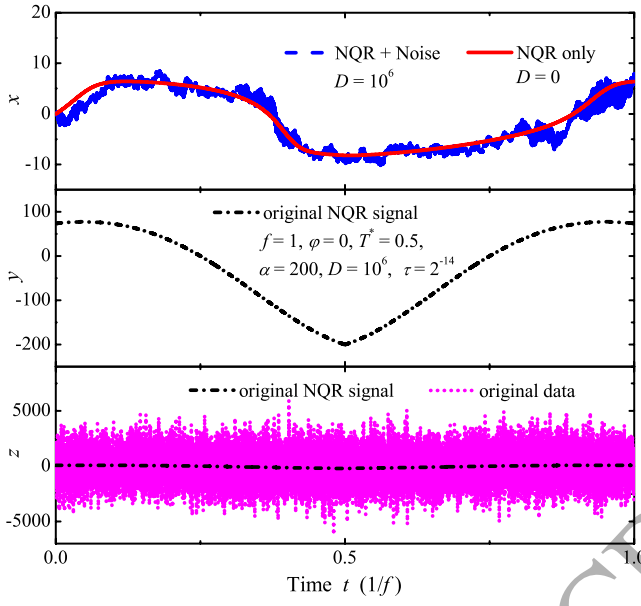

FIG. 1. (Color online) Simulation example (analog): An output waveform of an SR system (top row) and the corresponding input NQR signal (middle row) and original data (bottom row) with SNR=-38dB.

may cause serious confusion to NQR detection. Therefore, a companion algorithm is needed which can process the output data of SR system facilitating a valid NQR detection (see Subsection C).

B. SR circuit design

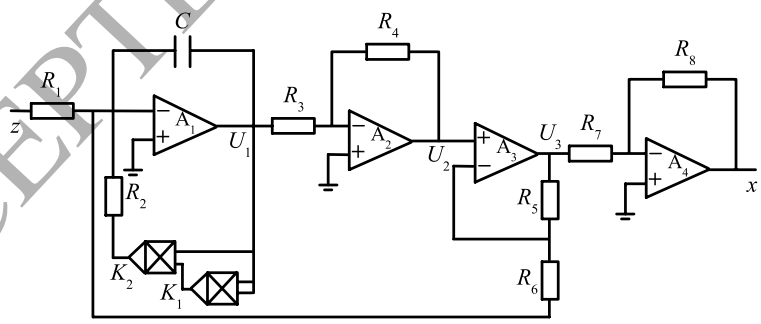

FIG. 2. Our SR circuit design.

As noted in the previous section, the SR system requires a hardware implementation, that is, a circuit which will transform the spectrometer output to a waveform with a resonant NQR signal. While this paper focusses on NQR detection assuming that the SR system can be implemented

successfully, we present in Fig. 2 a design of a possible SR-function circuit, to demonstrate that such a circuit can be easily constructed with simple electronics. For the circuit of Fig. 2 we have (see the Appendix for more details),

$$\begin{aligned} -C\frac{dU_1}{dt} &= \frac{z}{R_1} + \frac{K_1K_2U_1^3}{R_2} - \frac{R_4}{R_3R_6}U_1, \\ x = \Upsilon U_1 &= \frac{R_4R_8}{R_3R_7}\left(1+\frac{R_5}{R_6}\right)U_1. \end{aligned} \tag{7}$$

Denoting $\tilde{z} = -z$ and $\tilde{x} = R_1Cx/\Upsilon$ as the effective input and output, we have

$$\begin{aligned} \frac{d\tilde{x}}{dt} &= c_1\tilde{x} - c_2\tilde{x}^3 + \tilde{z}, \\ c_1 = \frac{R_4}{R_3R_6C}; &\quad c_2 = \frac{K_1K_2}{R_1^2R_2C^3}. \end{aligned} \tag{8}$$

In practice, it is important to control the output to input ratio (x/z). Our numerical experiments on Eq. (5) suggest that the output x and the NQR signal almost have "the same phase", that is, $\frac{dx}{dt}$=0 when $\left|\cos\left(2\pi\check{f}t+\varphi\right)\right|$ is about 1. Then, the output amplitude X approximately satisfies

$$X^3 - \frac{c_1}{c_2}X - \frac{\alpha}{c_2} = 0, \tag{9}$$

according to Eq. (5). If $\left(\frac{\alpha}{2c_2}\right)^2 \gg \left(\frac{c_1}{3c_2}\right)^3$, that is,

$$\alpha \gg 2c_1\sqrt{\frac{c_1}{27c_2}}, \tag{10}$$

a deep resonance will occur, and accordingly Eq. (9) has the unique solution

$$\begin{aligned} X = &\sqrt[3]{\frac{\alpha}{2c_2} + \sqrt{\left(\frac{\alpha}{2c_2}\right)^2 - \left(\frac{c_1}{3c_2}\right)^3}} \\ &+ \sqrt[3]{\frac{\alpha}{2c_2} - \sqrt{\left(\frac{\alpha}{2c_2}\right)^2 - \left(\frac{c_1}{3c_2}\right)^3}}. \end{aligned} \tag{11}$$

Then the X to α ratio can be adjusted by varying c_1 and c_2 in a real SR system design. A smaller c_2 yields larger X, but demands larger α (stronger NQR signal) for stronger resonance (see Eq. (10)). The value of c_1 should also be limited according to Eq. (10), but it is noted that smaller c_1 outputs lower resonance frequency (see Eq. (6)).

C. Overview of possible SR companion algorithms: AML, FSAML, and NN

As mentioned previously, the SR output signal must be processed by a detection/estimation algorithm in order to extract the NQR response. We designed our neural network (NN) as a quali-

fied companion algorithm for the SR approach. Other possible algorithms applied for this purpose include the previously proposed approximate maximum likelihood (AML) algorithm [7] and its frequency selective counterpart (FSAML) [8]. This section therefore presents the application of the AML, FSAML, and NN algorithms in conjunction with the SR approach. The combination of SR with AML or FSAML respectively results in the SRAML and SRFSAML methods.

1. The AML algorithm

Assume that the signal of interest (SOI) waveform is known and has an analytical expression $Aq(t;\mathbf{p})$, where A is the SOI amplitude and $\mathbf{p}$ is a vector of SOI's other parameters. The SOI can be identified from background noise based on approximate maximum likelihood (AML) theory [7]. Denoting the discrete NQR data by $\mathbf{Z}$, the N-points sampled $z(t)$ at sampling frequency f_s=$1/(t_1 - t_0)$ can be written as,

$$\begin{aligned}
&\mathbf{Z} = [z(t_0) \quad z(t_1) \quad \ldots \quad z(t_{N-1})]^{\mathrm{T}} = \alpha\mathbf{Q} + \mathbf{N},\\
&\mathbf{Q} = \left\{\cos\left(2\pi\check{f}t_i + \varphi\right)e^{-|t_i - t_{sp}|/T^*}\right\}_{N\times 1},\\
&\mathbf{p} = \left\{\check{f}, \varphi, T^*\right\},
\end{aligned} \tag{12}$$

where $\mathbf{N}$ is the discrete noise ($n(t)$), and $\mathbf{Q}$ is the discrete q of NQR signal, respectively. First, AML gets the amplitude estimation $\hat{A}$ based on the Least Square method,

$$\hat{A} = \mathbf{Q}^{\dagger}\mathbf{Z}, \tag{13}$$

where $(.)^{\dagger}$ denotes the Moore-Penrose pseudo-inverse. $\hat{A}$ is in fact a function of $\mathbf{p}$. Then AML defines the likelihood function L as

$$L(\mathbf{p}) = \mathbf{Z}^{\mathrm{H}}\mathbf{Q}\mathbf{Q}^{\dagger}\mathbf{Z}, \tag{14}$$

where $(.)^{\mathrm{H}}$ denotes the conjugate transpose. Maximizing L yields the estimation of $\mathbf{p}$,

$$\hat{\mathbf{p}} = \arg\max_{\mathbf{p}} L. \tag{15}$$

The search ranges of $\check{f}$ and T^* should cover all possible values which can be inferred from knowledge of the NQR parameters of the substance of interest [18], with φ within $[0, 2\pi)$. In particular, the search range of $\check{f}$ is the so-called "NQR band" which is a very narrow interval of possible

values around the known NQR resonance $\check{f}$. Once these featured parameters are estimated, they can be substituted into the AML test statistic [19],

$$T(\mathbf{Z}) = (2N-1)\frac{\mathbf{Z}^{\mathrm{H}}\mathbf{Q}\mathbf{Q}^{\dagger}\mathbf{Z}}{\mathbf{Z}^{\mathrm{H}}\mathbf{Z} - \mathbf{Z}^{\mathrm{H}}\mathbf{Q}\mathbf{Q}^{\dagger}\mathbf{Z}}, \tag{16}$$

which in fact can be interpreted as an estimation of the "NQR energy" to "noise energy" ratio, since $\mathbf{Z}^{\mathrm{H}}\mathbf{Q}\mathbf{Q}^{\dagger}\mathbf{Z}$ corresponds to NQR signal energy and $\mathbf{Z}^{\mathrm{H}}\mathbf{Z}$ is the energy of the total signal. Evidently, a larger T means a higher possibility of presence for the NQR signal. So, by predetermining a threshold value γ, the NQR signal is determined to be present if and only if $T>\gamma$, and otherwise not. To reduce false alarms, an effective detection algorithm should produce large T values when the NQR signal is present, and small ones otherwise.

Although it does not have an analytical expression, the SR system output $x(t)$ can preserve the main NQR features (see comparison of the plots in Fig.1), and therefore application of the AML algorithm to $x(t)$ should follow the same principles as in our previous analysis leading to Eq.(16). In fact, our numerical calculations show that $x(t)$ with an input containing an NQR signal is a periodic signal which fluctuates around a signal that resembles the NQR signal waveform (see again Fig.1, (a) and (b)). Therefore, we can follow a similar to the previous analysis to detect the SOI in $x(t)$, by setting,

$$\begin{aligned} \mathbf{p}_x &= \left\{\check{f}, \varphi_x, T^{**}\right\}, \\ q_x(t;\mathbf{p}_x) &\simeq \cos\left(2\pi\check{f}t + \varphi_x\right) e^{-|t-t_{sp}|/T^{**}}, \end{aligned} \tag{17}$$

where φ_x and T^{**} are in the same range as φ and T^{*}. Similar to Eq.(12), we have

$$\begin{aligned} \mathbf{X} &= [x(t_0) \quad x(t_1) \quad \ldots \quad x(t_{N-1})]^{\mathrm{T}} \simeq A_x\mathbf{Q}_x + \mathbf{N}_x, \\ \mathbf{Q}_x &= \left\{\cos\left(2\pi\check{f}t_i + \varphi_x\right) e^{-|t_i-t_{sp}|/T^{**}}\right\}_{N\times 1}, \end{aligned} \tag{18}$$

where $\mathbf{N}_x$ is the waveform fluctuation and $\mathbf{Q}_x$ is the approximation of the sampled $q_x(t;\mathbf{p}_x)$. Replacing $\mathbf{Z}$, $\mathbf{Q}$, and $\mathbf{p}$ in Eqs.(14), (15), and (16) with $\mathbf{X}$, $\mathbf{Q}_x$, and $\mathbf{p}_x$ yields the AML implementation for $x(t)$.

2. The FSAML algorithm

Both our numerical calculations (see Fig. 1) and theoretical analysis on Eq.(5) [16] illustrate that the SR output signal x is not a simple harmonic wave, but a nonlinear wave which contains $(2m+1)\check{f}$, $m = 0, 1, 2, \ldots$ frequency components. As the AML implementation using Eq.(18)

ignores the $m > 0$ components, these components in fact act as interference for AML processing. A way to ignore these components is by employing a well-known frequency selective variant of the AML algorithm, the FSAML, which combines the AML algorithm with a frequency selective (FS) method [8]. By implementing a simple Discrete Fourier transformation (DFT), the FS method can select the frequency components inside the NQR band and exclude all other frequency components. This can be achieved by dividing the NQR band in a vector of J subbands, $[f_{s1} \quad f_{s2} \quad ... \quad f_{sJ}]$. Then, a DFT for $\mathbf{X}$ and $\mathbf{Q}_x$ yields

$$\begin{aligned}
&\left(\widetilde{\mathbf{X}}, \widetilde{\mathbf{Q}}_x\right) = \mathbb{V}_J\left(\mathbf{X}, \mathbf{Q}_x\right), \\
&\mathbb{V}_J = \begin{pmatrix} 1 & e^{-j2\pi f_{s1}/f_s} & .. & e^{-j2\pi(N-1)f_{s1}/f_s} \\ 1 & e^{-j2\pi f_{s2}/f_s} & .. & e^{-j2\pi(N-1)f_{s2}/f_s} \\ .. & .. & .. & .. \\ 1 & e^{-j2\pi f_{sJ}/f_s} & .. & e^{-j2\pi(N-1)f_{sJ}/f_s} \end{pmatrix},
\end{aligned} \tag{19}$$

where f_s is the sampling frequency. $\widetilde{\mathbf{X}}$ contains only the frequency domain information within NQR band, eliminating $(2m+1)\check{f}$, $m = 1, 2, ...$ frequency components. Combining this method with AML yields the FSAML likelihood function and test statistic for $\mathbf{X}$,

$$\begin{aligned}
&\widetilde{L}\left(\check{f}, T^{**}, \varphi_x\right) = \widetilde{\mathbf{X}}^{\mathrm{H}}\widetilde{\mathbf{Q}}_x\widetilde{\mathbf{Q}}_x^{\dagger}\widetilde{\mathbf{X}}, \\
&\widetilde{T}\left(\widetilde{\mathbf{X}}\right) = (2J-1)\frac{\widetilde{\mathbf{X}}^{\mathrm{H}}\widetilde{\mathbf{Q}}_x\widetilde{\mathbf{Q}}_x^{\dagger}\widetilde{\mathbf{X}}}{\widetilde{\mathbf{X}}^{\mathrm{H}}\widetilde{\mathbf{X}} - \widetilde{\mathbf{X}}^{\mathrm{H}}\widetilde{\mathbf{Q}}_x\widetilde{\mathbf{Q}}_x^{\dagger}\widetilde{\mathbf{X}}}.
\end{aligned} \tag{20}$$

We denote the combination of SR with AML (or FSAML), as SRAML (or SRFSAML), and test their performance for NQR detection in numerical calculations in the next section.

3. *The NN approach*

Beyond conventional mathematical methods such as AML and FSAML, we can also apply neural network theory to discern the features of $\mathbf{X}$. As neural networks are able to approximate or distinguish arbitrary functions, we expect this approach to be better suited given that $\mathbf{X}$ is a complex nonlinear waveform which has no analytical expression.

The NN approach considers a single "neuron" which receives information values u_i from M channels, and generates a value U,

$$U = \sum_{i=1}^{M} w_i u_i, \tag{21}$$

where w_i is the weight coefficient of the i-th channel. The values of w_i are chosen to ensure that, as the object information travels through the channels, the generated value U correctly matches the class of the tested object. U can take any real number according to Eq. (21), but should be within a specific range to improve robustness. For this reason, a so-called activation function is introduced to project U to a finite interval, such as the sigmoid function,

$$v = F(U) = \frac{1}{1 + e^{-U}}, \tag{22}$$

which projects U to the $[0, 2]$ interval ($v\epsilon[0, 2]$).

Suppose there are L samples with their information vector being $\mathbf{u}_I = [u_1, u_2, ..., u_M]^{\mathrm{T}}$, $I = 1, 2, ..., L$. The trained neuron should have a set of weighting factors w_i (forming the vector $\mathbf{w} = [w_1, w_2, ..., w_M]^{\mathrm{T}}$) which satisfy,

$$F(\mathbf{u}_I^{\mathrm{T}}\mathbf{w}) = v_I, \quad I = 1, 2, ..., L, \tag{23}$$

where each v_I is equal to the unique value corresponding to the class of the I-th sample. However, usually Eq. (23) cannot be satisfied strictly, and we can only find $\mathbf{w}$ which yields a minimal global error $ee_{\min}$,

$$ee_{\min} = \min_{\mathbf{w}} \left\| \mathbf{v} - F([\mathbf{u}_1 \quad \mathbf{u}_2 \quad ... \quad \mathbf{u}_L]^{\mathrm{T}}\, \mathbf{w}) \right\|_2^2, \tag{24}$$

where $\mathbf{v} = [v_1, v_2, ..., v_L]^{\mathrm{T}}$. For any object with information $\mathbf{u}$, classification is made by substituting the acquired $\mathbf{w}$ into Eq. (21) and finding out which class value is the closest to the generated value v. The ability of a single neuron is very limited. If several neurons form a neuron layer and several layers constitute a big 3D net, however, this neural network can deal with extremely complicated tasks related to classification, recognition, strategic decision, etc.

4. NN implementation

To implement the NN approach, we train feedforward neural networks [20] using the corresponding Matlab toolbox. To do this, we simulate N_s Monte Carlo samples of NQR signal plus Gaussian white noise as well as N_s Monte Carlo samples of pure Gaussian white noise, and calculate the corresponding sampled SR output $\mathbf{X}$ as training samples. These two classes of $\mathbf{X}$ are respectively marked as $\mathbf{X}_i^{(p)}$ and $\mathbf{X}_i^{(s)}$, $i = 1, 2, ..., N_s$. The network is expected to generate v=1 if $\mathbf{X}_i^{(p)}$ is the information vector and v=0 otherwise. There is one middle layer containing 10 neurons between the input and output ports of our network. Our numerical tests have suggested that this

TABLE I. Our discussed methods

METHOD	WORKFLOW [$z(t)$: NQR data; T: test statistic]
AML	$z(t) \xrightarrow{\text{sampling}} \mathbf{Z} \xrightarrow{\text{AML}} T(\mathbf{Z})$.
SRAML	$z(t) \xrightarrow{\text{SR system}} x(t)$; $x(t) \xrightarrow{\text{sampling}} \mathbf{X} \xrightarrow{\text{AML}} T(\mathbf{Z})$.
SRFSAML	$z(t) \xrightarrow{\text{SR system}} x(t)$; $x(t) \xrightarrow{\text{sampling}} \mathbf{X} \xrightarrow{\text{frequency selective}} \widetilde{\mathbf{X}}$; $\widetilde{\mathbf{X}} \xrightarrow{\text{AML}} \widetilde{T}\left(\widetilde{\mathbf{X}}\right)$.
NN	$z(t) \xrightarrow{\text{sampling}} \mathbf{Z} \xrightarrow{\text{neural network}} T_{net}(\mathbf{Z})$.
SRNN	$z(t) \xrightarrow{\text{SR system}} x(t)$; $x(t) \xrightarrow{\text{sampling}} \mathbf{X} \xrightarrow{\text{neural network}} T_{net}(\mathbf{X})$.

network size is sufficient to implement our SRNN approach successfully for the datasets considered in this work. The activation function for the trained network is the sigmoid function defined in Eq. (22). The network weight coefficients are calculated by searching for the minimal global error using the Levenberg-Marquardt backpropagation method [21]. This trained network can be invoked for analyzing practical data in Matlab. For any sampled SR system output $\mathbf{X}$, the network can output a value marked as $T_{net}(\mathbf{X})$. T_{net} is in fact the neural network test statistic like those in Eqs. (16) and (20), by predetermining a threshold value γ_{net}, the NQR signal is deemed present if and only if $T_{net}(\mathbf{X})>\gamma_{net}$, and otherwise not.

Please note that similarly one can also train a neural network for processing sampled NQR data $\mathbf{Z}$ using Monte Carlo samples: $\mathbf{Z}_i^{(p)}$, NQR signal plus Gaussian white, and $\mathbf{Z}_i^{(s)}$, pure Gaussian white noise, $i = 1, 2, ..., N_s$.

Table I presents a "workflow" of the steps involved in each of the considered AML, SRAML, SRFSAML, NN, and SRNN methods, from which the similarities and differences of each method can be easily derived.

III. NUMERICAL ANALYSIS ON THE PERFORMANCE OF THE SRNN METHOD

This section presents numerical results to assess the performance of the SRNN method. The results by AML, NN algorithms, and SRAML, SRFSAML methods are also presented as comparison.

The frequency of NQR signal is usually located in the radio frequency band (MHz). However, a simple modulation can center its spectrum around zero so that it can easily meet the resonance condition in Eq. (6) of an SR system. Then the real frequency band of the recorded data is $[f_c - f_s/2, f_c + f_s/2]$, where f_c denotes the frequency center of our signal modulation, and f_s is the sampling frequency of the spectrometer for recording data.

If we choose the ^{14}N in sodium nitrite ($NaNO_2$) as the NQR signal source, the NQR frequency $\check{f}$ and damping time T^* are respectively about 1MHz and 1ms in our lab environment according to NQR theory. By setting f_s=1/(16μs) and N=128 sampling points per echo, and f_c= 0.9995MHz$\simeq \check{f} - f_s/N$, the whole echo time is approximately one cycle of the NQR signal. The noise fluctuation time τ (normally ranging from 1ns to 1μs as mentioned before) is assumed to be $2^{-7}/f_s = 0.125\mu$s without loss of generality.

For the ease of numerical analysis, we normalize the time and the signal amplitude, so that $\widetilde{t} = tf_s/N \in [0, 1)$. Then $\widetilde{\check{f}} = \check{f}N/f_s = 1$, $\widetilde{T^*} = T^* f_s/N \simeq 0.5$, and c_1 and c_2 in Eq. (5) become $\widetilde{c_1} = c_1 N/f_s$ and $\widetilde{c_2} = c_2 N/f_s$, respectively. In the following numerical simulations, for our preference and convenience, the amplitude α of NQR signal is normalized to be 200. The parameters of our SR system are as in Fig. 1 and the SR parameters are $\widetilde{c_1} = 10$ and $\widetilde{c_2} = 0.5$. Please note one may of course make a different normalization.

A. Training a neural network for a specific NQR signal

We created a simulated analog data set of 1000 Monte Carlo runs for a specific NQR signal and stochastic noise with parameters detailed in the previous section and in Fig.1. The AML and NN algorithms use the sampling vector $\mathbf{Z} = [z(t_0) \quad z(t_1) \quad ... \quad z(t_{N-1})]^{\mathrm{T}}$ from these data z as input. The SRAML, SRFSAML, and SRNN methods use the sampling output ($\mathbf{X}$) of the SR system with its input being the original simulated data z.

To train our neural network, we use the same process to additionally create 100 Monte Carlo runs of data as training samples. In the SRNN method, the neural network is trained to specif-

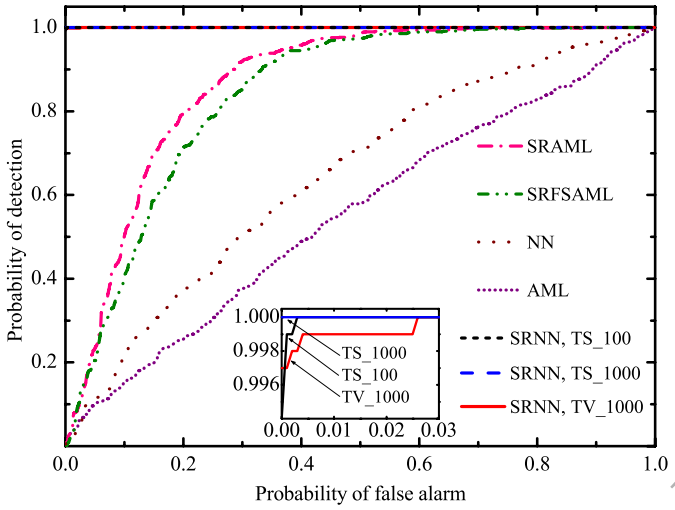

FIG. 3. (Color online) The ROC curves obtained by SRAML, SRFSAML, NN, AML, and SRNN for the case of Fig. 1, where $(\widetilde{f}, \varphi, \widetilde{T^*}, \alpha, D)$=(1, 0, 0.5, 200, 10^6) with SNR=-38dB.

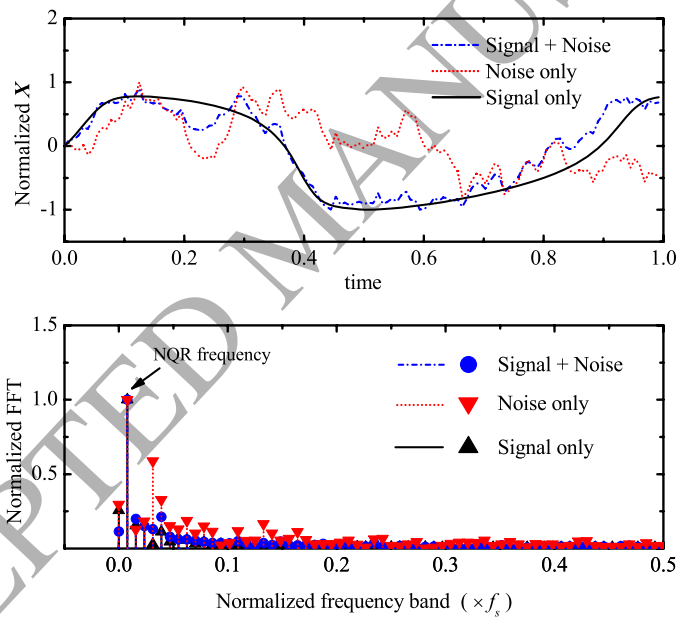

FIG. 4. (Color online) The waveforms of normalized **X** corresponding to SR system input of NQR signal only, Noise only, and NQR signal + Noise, as well as their normalized spectra from a Monte Carlo run of simulated data, where $(\widetilde{f}, \varphi, \widetilde{T^*}, \alpha, D)$=(1, 0, 0.5, 200, 10^6) with SNR=-38dB.

ically analyze the SR system output, so that the training samples are grouped in vector **X**. For comparison, we also consider a pure neural network (NN) algorithm which tries to analyze the original data directly, and therefore considers **Z** as the training samples vector. The trained neural

network in SRNN is marked as "TS-100" where "TS" means "train for specific". To compare performance with a case of more training samples, we also created data using 1000 Monte Carlo runs and trained another network marked as "TS-1000". Evidently, a neural network which learns from more samples should be more "experienced" and exhibit better performance.

Figure 3 shows the receiver operating characteristic (ROC) curves of AML, NN, SRAML, SRFSAML, and SRNN. The SNR of these data is -38dB (see Eq.(3)), which as we can see is low enough to cause the AML algorithm to fail. On the contrary, the SRNN method has an almost perfect detection performance for the NQR signal, and the SRNN implementation with more training samples ("TS-1000") outputs perfect results. The plot also confirm that the application of AML after applying SR theory (SRAML) performs better than plain AML or even NN methods. However, SRAML can not match SRNN in performance, as the neural network approach is more effective than traditional mathematical methods such as AML in discerning complicated waveforms.

Interestingly, SRAML performs better than its frequency selective counterpart, SRFSAML, which is counter-intuitive and thus worth investigating. To illustrate this point, we have plotted a specific example of possible SR outputs $\mathbf{X}$ for "NQR signal + noise" and "noise only" signals in Fig.4. As shown in this figure, the SR output for "noise only" data is indeed random and irregular relative to "NQR signal + noise" data, but contains a strong component coinciding with the NQR frequency $\widetilde{f}$. This strong frequency component will be selected by SRFSAML and may be regarded as an NQR signal feature resulting in a false alarm. Therefore, applying a frequency selection method in SR outputs does not guarantee a better performance in all cases. Contrary to SRFSAML, SRAML is not affected by this frequency component as it operates directly in the time domain.

These results suggest that conventional detection methods are not able to deal with the complicated SR system output $\mathbf{X}$, while neural networks can discern the subtle features of $\mathbf{X}$ effectively. The poor performance of the plain NN algorithm is also worth noting, which confirms that a pure neural network is not very efficient for detecting signals with very low SNR, unless it is combined with the SR method proposed in this paper.

B. Training a neural network for a variety of NQR signals

The neural network in the previous subsection was trained to discern only a specific SR waveform of a NQR signal with fixed parameters. Its usefulness is therefore limited to cases where the

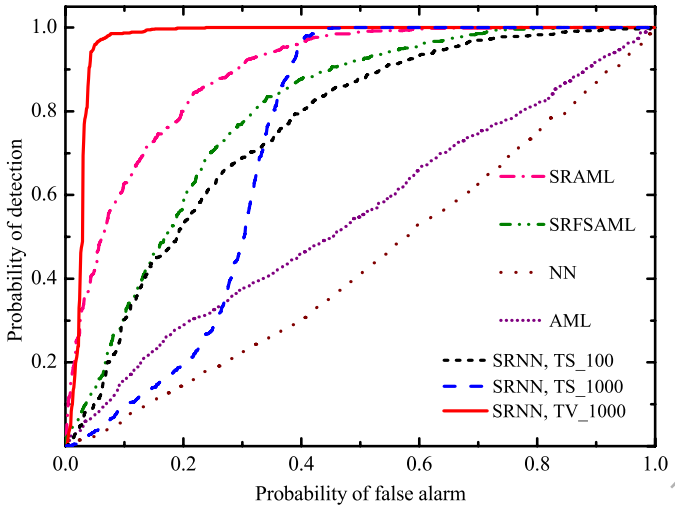

FIG. 5. (Color online) The ROC curves obtained by SRAML, SRFSAML, NN, AML, and SRNN for the case $(\widetilde{f}, \varphi, \widetilde{T^*}, \alpha, D)$=(1.1, $\pi/3$, 0.5, 200, 10^6) with SNR=-38dB.

TABLE II. NQR parameter ranges

Frequency $\widetilde{f}$	(0.5, 2.0)
Initial phase φ	$[0, 2\pi)$
Damping time $\widetilde{T^*}$	$\geq$ 0.5 (or a bit smaller)
Amplitude α	$\geq$ 200 (or a bit smaller)
Noise variance D	$\leq 10^6$ (or a bit larger)

NQR signal's parameters are known exactly. It is important, therefore, to train a neural network which is suitable for NQR data with parameters that are within certain ranges. The ranges for our (dimensionless) parameters of interest are shown in "TABLE II". To train the corresponding neural network, we create 1000 Monte Carlo analog samples of stochastic noise with $D = 10^6$, and NQR signal with frequency $\widetilde{f}$ and initial phase φ that are randomly picked from the intervals $(0.5, 2)$ and $[0, 2\pi)$, respectively, and with an amplitude α of 200, and a damping time $\widetilde{T^*}$ of 0.5 (for each Monte Carlo sample). These data pass through the SR system yielding the related $\mathbf{X}$ as the sample data. We mark this neural network as "TV-1000" where "TV" means "train for a variety of NQR signals".

Figure 5 shows the ROC curves of our simulated case. It is clear that "TS-100" and "TS-1000" cannot deal with the NQR signal in this case, although this case is very similar with that in last subsection except for small differences for $\widetilde{f}$ and φ. Comparing Fig. 3 with Fig. 5, it is clear that

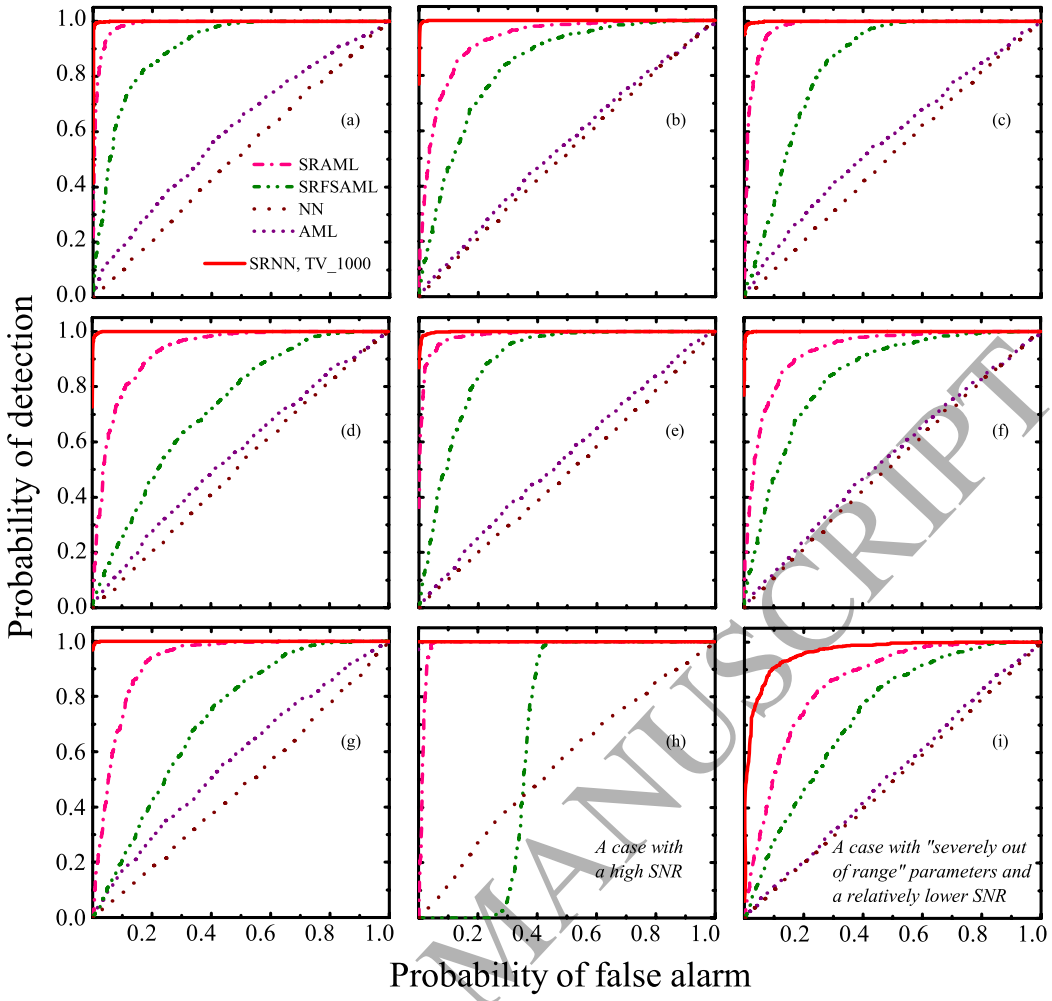

FIG. 6. (Color online) The ROC curves obtained by SRAML, SRFSAML, NN, AML, and SRNN for 9 representive cases. For the parameters ($\widetilde{f}$, φ, $\widetilde{T^*}$, α, D) and the corresponding SNR, case (a): (0.61, 0.94π, 1.63, 220, 0.9×10^6) and -30dB, case (b): (1.95, $\pi/10$, 1.2, 250, 1.2×10^6) and -31dB, case (c): (0.89, 0.48π, 20, 175, 1.35×10^6) and -35dB, case (d): (1.7, $5\pi/3$, 1, 200, 1.2×10^6) and -36dB, case (e): (0.55, 0.22π, 0.6, 190, 1.1×10^6) and -39dB, case (f): (1.33, 1.83π, 0.7, 170, 1.1×10^6) and -40dB, case (g): (0.72, $2\pi/3$, 0.4, 180, 1.2×10^6) and -43dB, case (h): (0.53, 0.89π, 10, 800, 0.5×10^6) and -0.38dB, case (i): (1.15, 1.21π, 0.45, 160, 1.5×10^6) and -46dB.

these two "TS" networks retain specificity for a given NQR signal but ignore any other pattern. In other words, they sacrifice commonality for pursuing extremely high precision in handling their specificity. Compared to "TS-100", "TS-1000" is trained with more samples so that it is more concentrated to its specific NQR signal, and it has better performance (the perfect performance) in Fig. 3 (see the subgraph). Accordingly, "TS-1000" is poorer than "TS-100" in dealing with the

case in Fig. 5. Compared to the two "TS" nets, "TV-1000" has good performance in both two cases. However, it is slightly poorer than the two "TS" nets in Fig. 3 (see the subgraph). This can be understood as "TV-1000" should concentrate on more than one NQR signal, thereby sacrificing some accuracy.

In order to further test the commonality of "TV-1000", we have considered various sets of NQR parameters within the ranges of "TABLE II", and respectively created 1000 Monte Carlo data for each set to be processed by "TV-1000". Our numerical results indicate that the trained neural network can handle well all these different cases. Some representative cases are shown in Fig. 6, which constitute a wide variety of NQR data parameters within the ranges of "TABLE II". It is apparent that "TV-1000" is very robust with respect to these low SNR cases. As the SNR is gradually reduced from cases (a) to (g), its performance remains "close to perfect". The figure also suggests that SNR and network performance do not have an exact linear relationship. Apart from the SNR level, the network is also sensitive to the specific parameters of a case. When the parameters are significantly out of range and the SNR is reduced considerably, the performance of the trained network will eventually degrade, as illustrated in case (i) of Fig.6.

The numerical results of "TV-1000" suggest that it is possible to train a high perfomance and good commonality neural network coupled with an SR system facilitating good NQR detection. Our experience of training "TV-1000" is that: I) $\widetilde{f}$ and φ should randomly vary among the samples; II) it is preferable to assign the lowest value for the SNR of the sample data that can be tolerated by the network, as the trained network can handle any NQR data of higher SNR (see for example case (h) with SNR=-0.38dB in Fig. 6). This means that one should choose the amplitude α and the damping time $\widetilde{T^*}$ to be their minimum, and the noise variance D to be its maximum. Following these guidelines, one can train a neural network for NQR detection of other parameter domains. The network for our SRNN method can be trained using samples based on numerical simulations, and then be applied to experimental data. Alternatively, it could be trained with experimental data in controlled laboratory conditions before being tested in realistic practical applications where low SNRs pose a great detection challenge, such as humanitarian demining.

C. Training a neural network for NQR signals in the presence of strong interference

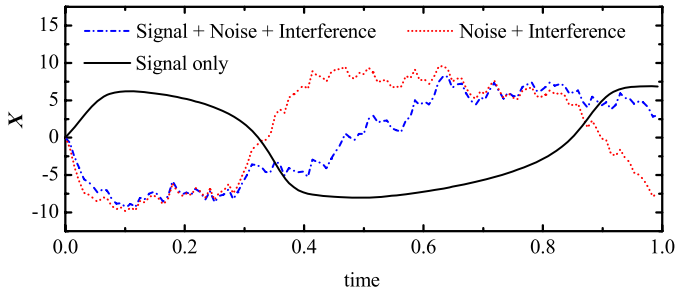

FIG. 7. (Color online) The waveforms of **X** corresponding to SR system input of NQR signal only, Noise + Interference, and NQR signal + Noise + Interference from a Monte Carlo run of test data, where ($\widetilde{f}$, φ, $\widetilde{T^*}$, α, D)=(0.97, 0.11, 0.7, 185, 1.4×10^6) with SNR=-40dB.

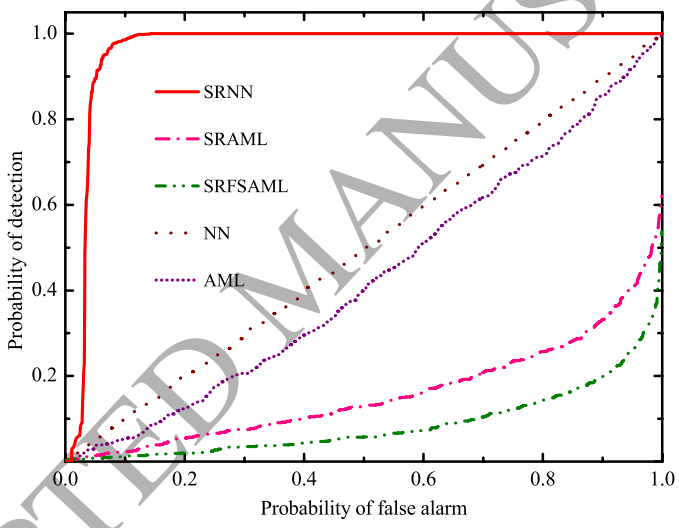

FIG. 8. (Color online) The ROC curves obtained by SRAML, SRFSAML, NN, AML, and SRNN for the interference case, where ($\widetilde{f}$, φ, $\widetilde{T^*}$, α, D)=(0.97, 0.11, 0.7, 185, 1.4×10^6) with SNR=-40dB.

Interference may be a severe problem in real-life NQR detection [9, 10]. It is therefore necessary to train a network which can deal with strong interference in addition to low SNRs, adding another level of complexity relative to detecting "NQR signal + noise" cases. Modifying the SRNN algorithm to account for arbitrary interference is beyond the scope of this paper. We present, however, a preliminary analysis for scenarios where the properties of the background interference are already known. In these situations, our numerical simulations suggest good performance for the proposed SRNN method, as illustrated in the following example.

Suppose the interference $r\left(\widetilde{t}\right)$ contains two harmonic components. We consider the challenging situation that both these components are located within an assumed NQR band $\widetilde{\widetilde{f}} \in [-0.9, 1.1]$ which leads to a severe overlapping spectrum with the NQR signal. Moreover, the interference is assumed deterministic and sufficiently strong to obscure the NQR signal, which is given by the formula below,

$$\begin{aligned} r\left(\widetilde{t}\right) &= 250\cos\left(2\pi\widetilde{f_1}\widetilde{t} + \frac{2\pi}{3}\right) + 250\cos\left(2\pi\widetilde{f_2}\widetilde{t} + \frac{6\pi}{5}\right), \\ \widetilde{f_1} &= 1.0, \quad \widetilde{f_2} = 1.05. \end{aligned} \tag{25}$$

Regarding the training samples (1000 Monte Carlo), $\widetilde{\widetilde{f}} \in [-0.9, 1.1]$, the other parameters φ, $\widetilde{T^*}$, α, and D are referred to TABLE II. Training our network for this case is based on our experience of training "TV-1000" (see the last paragraph of Section III.B). The parameters of the test data are chosen as ($\widetilde{\widetilde{f}}$, φ, $\widetilde{T^*}$, α, D)=(0.97, 0.11, 0.7, 185, 1.4×10^6) with SNR=-40dB. We have set the interference in the test data to be slightly different from that of the training samples, as a priori knowledge of the interference parameters can never be perfect. The interference in the test data can therefore be written as,

$$\begin{aligned} r\left(\widetilde{t}\right) &= 245\cos\left(2\pi\widetilde{f_1}\widetilde{t} + \frac{1.91\pi}{3}\right) + 260\cos\left(2\pi\widetilde{f_2}\widetilde{t} + \frac{6.1\pi}{5}\right), \\ \widetilde{f_1} &= 0.97, \quad \widetilde{f_2} = 1.07. \end{aligned} \tag{26}$$

We specifically set $\widetilde{f_1}$=$\widetilde{\widetilde{f}}$ so that the NQR signal coincides with the f_1 interference component in order to challenge our trained network. The trained neural network is able to identify the existence of the NQR signal (see Fig. 8) despite being obscured by the strong interference present in the signal, as shown in Fig.7. We note that SRAML and SRFSAML are incapable of processing this interference case, since both the **X** with and without NQR response contain distinct NQR-frequency harmonic components which in fact are due to interference. In fact, in this case, the harmonic component in **X** with NQR response looks weaker than that in **X** without NQR response (see Fig.7), which can explain why the ROC curves of SRAML and SRFSAML are beneath the diagonal line, in agreement with the physical interpretation of Eq.(16).

We have further tested the robustness of the trained network in various cases of $\widetilde{\widetilde{f}}$, φ, $\widetilde{T^*}$, α, D, and have obtained good results in all cases using our SRNN approach. To deal with situations of very complicated interference with unknown properties, a more complex network containing more neurons and layers and trained with more samples is needed; this challenging research topic will

be addressed in our future work. Moreover, some of our preliminary results suggest it may also be possible to combine our SRNN method with our interference cancellation method presented in [9] in order to deal with cases of strong interference and very low SNRs; a detailed analysis of this approach is beyond the scope of this work and will be presented in a subsequent paper.

IV. CONCLUSION

This paper proposes a method for detecting extremely weak NQR signals, termed SRNN, which combines stochastic resonance with neural network. A stochastic resonance system is suitably designed and simulated, which can lead to a nonlinear waveform that features a resonant NQR signal together with stochastic noise. A feedforward neural network is applied specifically to this special nonlinear waveform, allowing to identify the NQR signal more accurately than traditional detection methods. When the signal to noise ratio is so low that other detection methods or algorithms (including a pure neural network) cannot detect the NQR signal of interest, the SRNN approach can remedy this situation and lead to accurate NQR detection. By proper training, the neural network in SRNN can have good commonality, and is suitable for detecting any NQR signal whose parameters are within certain ranges. Our preliminary work has also shown that SRNN is also effective in cases of strong interference with known features, which includes a strong NQR frequency component. Based on these encouraging results, we anticipate that the proposed SRNN method can be applicable to other problems of detecting weak signals under a similar framework.

V. APPENDIX

Eq. (5) can be solved using the following strategy.

$$
\begin{aligned}
k_{11} &= c_1 x|_{t=2l\tau} - c_2 \left(x|_{t=2l\tau}\right)^3 + z|_{t=2l\tau}, \\
k_{13} &= c_1 \left(x|_{t=2l\tau} + \tau k_{12}\right) - c_2 \left(x|_{t=2l\tau} + \tau k_{12}\right)^3 + z|_{t=(2l+1)\tau}, \\
k_{14} &= c_1 \left(x|_{t=2l\tau} + 2\tau k_{13}\right) - c_2 \left(x|_{t=2l\tau} + 2\tau k_{13}\right)^3 + z|_{t=(2l+2)\tau}, \\
x|_{t=(2l+2)\tau} &= x|_{t=2l\tau} + \tau \left(k_{11} + 2k_{12} + 2k_{13} + k_{14}\right)/3, \\
k_{21} &= c_1 x|_{t=(2l+1)\tau} - c_2 \left(x|_{t=(2l+1)\tau}\right)^3 + z|_{t=(2l+1)\tau}, \\
k_{22} &= c_1 \left(x|_{t=(2l+1)\tau} + \tau k_{21}\right) - c_2 \left(x|_{t=(2l+1)\tau} + \tau k_{21}\right)^3 + z|_{t=(2l+2)\tau}, \\
k_{23} &= c_1 \left(x|_{t=(2l+1)\tau} + \tau k_{22}\right) - c_2 \left(x|_{t=(2l+1)\tau} + \tau k_{22}\right)^3 + z|_{t=(2l+2)\tau}, \\
k_{24} &= c_1 \left(x|_{t=(2l+1)\tau} + 2\tau k_{23}\right) - c_2 \left(x|_{t=(2l+1)\tau} + 2\tau k_{23}\right)^3 + z|_{t=(2l+3)\tau}, \\
x|_{t=(2l+3)\tau} &= x|_{t=(2l+1)\tau} + \tau \left(k_{21} + 2k_{22} + 2k_{23} + k_{24}\right)/3,
\end{aligned}
$$

where $l = 0, 1, 2, ...$, and the initial condition for this strategy is set to be $x(0)$=0 and $x(1)$=$x(0)$ + $\tau[c_1 x(0) - c_2 x^3(0) + z(0)]$.

Based on Kirchhoff's law and the properties of operational amplifier and multiplier, we have the following equation set.

$$
\begin{aligned}
&I_1 = \frac{z}{R_1}, \quad I_2 = \frac{K_1 K_2 U_1^3}{R_2}, \\
&I_6 = \frac{U_2}{R_6} = \frac{U_3 - U_2}{R_5} = -\frac{U_3}{R_7} = \frac{x}{R_8}, \\
&I_C = -C\frac{dU_1}{dt} = \frac{U_1}{R_3} = -\frac{U_2}{R_4}, \\
&I_1 + I_2 + I_6 = I_C,
\end{aligned}
$$

where I_i and I_C respectively denote the currents through resistor R_i and capacitor C. Then Eq. (7) can be obtained by solving this set.

ACKNOWLEDGMENT

This work has been supported by Find a Better Way (FABW) UK, under Project AQUAREOS.

[1] J. A. S. Smith, "Nuclear quadrupole resonance spectroscopy," *J. Chem. Educ.*, vol. 48, no. 1, pp. 39–48, 1971.

[2] N. R. Butt, E. Gudmundson, and A. Jakobsson, "An overview of NQR signal detection algorithms," in *Magnetic Resonance Detection of Explosives and Illicit Materials*, ser. NATO Science for Peace and Security Series B: Physics and Biophysics, T. Apih, B. Rameev, G. Mozzhukhin, and J. Barras, Eds. Springer, 2013, pp. 19–34.

[3] J. Barras, D. Murnane, K. Althoefer, S. Assi, M. D. Rowe, I. Poplett, G. Kyriakidou, and J. A. S. Smith, "Nitrogen-14 nuclear quadrupole resonance spectroscopy: a promising new analytical methodology for medicines authentication and counterfeit antimalarial analysis," *Analytical Chemistry*, vol. 84, pp. 2746–2753, 2013.

[4] J. Barras, K. Althoefer, M. D. Rowe, I. Poplett, and J. A. S. Smith, "The emerging field of nuclear qudrupole resonance-based medicines authentication," *Appl. Magn. Reson.*, vol. 43, pp. 511–529, 2012.

[5] M. D. Rowe and J. A. S. Smith, "Mine detection by nuclear quadrupole resonance," *in Proc. EUREL Int. Conf. on the Detection of Abandoned Land Mines*, pp. 62–66, Oct. 1996.

[6] A. Gregorovič and T. Apih, "Relaxation during spin-lock spin-echo pulse sequence in n 14 nuclear quadrupole resonance," *J. Chem. Phys.*, vol. 129, p. 214504, 2008.

[7] A. Jakobsson, M. Mossberg, M. D. Rowe, and J. A. S. Smith, "Exploiting temperature dependency in the detection of nqr signals," *IEEE Transactions on Signal Processing*, vol. 54, no. 5, pp. 1610–1616, 2006.

[8] ——, "Frequency-selective detection of nuclear quadrupole resonance signals," *Journal of Pharmaceutical and Biomedical Analysis*, vol. 43, no. 11, pp. 2659–2665, 2005.

[9] W. H. Shao, J. Barras, K. Althoefer, and P. Kosmas, "Detecting nqr signals severely polluted by interference," *Signal Processing*, vol. 138, pp. 256–264, 2017.

[10] W. Shao, J. Barras, P. Kosmas, and K. Althoefer, "The use of wavelets basis for cancelling time-varying interference in nqr signal detection," *submitted to IEEE Transactions on Signal Processing*.

[11] D. Gong, G. Hu, X. Wen, C. Yang, G. Qin, R. Li, and D. Ding, "Experimental study of the signal-to-noise ratio of stochastic resonance systems," *Phys. Rev. A*, vol. 46, pp. 3243–3249, 1992.

[12] G. P. Harmer, B. R. Davis, and D. Abbott, "A review of stochastic resonance: circuits and measurement," *IEEE Transactions on Instrumentation and Measurement*, vol. 51, pp. 299–309, 2002.

[13] D. J. C. MacKay, *Information Theory, Inference, and Learning Algorithms*. Cambridge University Press, 2003.

[14] S. D. Somasundaram, A. Jakobsson, J. A. S. Smith, and K. Althoefer, "Exploiting spin echo decay in the detection of nuclear quadrupole resonance signals," *IEEE Trans. Geosc. Remote Sensing*, vol. 45, pp. 925–933, 2007.

[15] A. S. Asdi and A. H. Tewfik, "Detection of weak signals using adaptive stochastic resonance," *Acoustics, Speech, and Signal Processing, 1995. ICASSP-95., 1995 International Conference on.*

[16] H. Risken, *The Fokker Planck Equation*. Springer Verlag, Berlin, 1984.

[17] K. Huang, *Statistical Mechanics*. Cambridge: Massachusetts, 1963.

[18] S. D. Somasundaram, "Advanced signal processing algorithms based on novel nuclear quadrupole resonance models for the detection of explosives," Ph.D. dissertation, King's College London, 2007.

[19] S. M. Kay, *Fundamentals of Statistical Signal Processing, Volume II: Detection Theory*. Englewood Cliffs, NJ: Prentice-Hall, 1998.

[20] G. Bebis and M. Georgiopoulos, "feed-forward neural networks," *IEEE Potentials*, vol. 13, pp. 27–31, 1994.

[21] K. Levenberg, "A method for the solution of certain non-linear problems in least squares," *Quarterly of Applied Mathematics*, vol. 2, pp. 164–168, 1944.